



A two-dimensional numerical model of a planar solid oxide fuel cell

Norouz Mohammad Nouri^{*}, Amin Mirahmadi, Majid Kamvar

Department of Mechanical Engineering, Iran University of Science and Technology (IUST), Tehran, Iran

Received 1 October 2010; received in revised form 26 November 2010; accepted 27 November 2010

Abstract

A two-dimensional CFD model of a planar solid oxide fuel cell (SOFC) has been developed. This model can predict the performance of SOFC at various operating and design conditions. The effect of Knudsen diffusion is accounted in the porous electrode (backing) and reaction zone layers. The mathematical model solves conservation of electrons and ions and conservation of species. The model is formulated in COMSOL Multiphysics 3.4, a commercial Finite Element Method (FEM) based on software package. The objective of the present study is to compare the results obtained from FEM with Control Volume Method (CVM) results obtained by Hussain et al. Both sets of results are compared with the experimental data published in literature. The results obtained by FEM show more accurate agreement with the experimental data. Finally, the effect of various operating and design parameters on the performance of SOFC has been examined.

Keywords: Solid oxide fuel cell; Reaction zone layers; Modeling; COMSOL Multiphysics.

1. Introduction

A conventional solid oxide fuel cell consists of two electrodes (i.e. an anode and a cathode, both of which are porous), and an electrolyte (which is non-porous, and sandwiched between the two electrodes). Conventional solid oxide fuel cells (SOFCs) are operated in temperature range of 700-1000°C [1]. Due to flexibility in fuel choice, SOFCs are receiving considerable attention for both small- and large-scale applications [1]. SOFCs can operate directly on hydrocarbon fuels with or without internal reforming, thereby reducing the cost of an external reformer [2]. Hence, fuel flexibility is one of the greatest advantages of SOFCs as compared to other types of fuel cells.

The planar-type design of SOFCs has the potential to offer higher power density than the tubular design [1]. Due to its compactness, it can be stacked in resemblance to polymer electrolyte membrane (PEM) fuel cells to satisfy the power requirement of an application [1]. Higher power density of planar SOFC is due to the shorter current paths resulting in low ohmic overpotential [3]. Moreover, planar SOFC is simple to fabricate and can be manufactured into various configurations [3]. However, this high temperature requirement limits the applicability of SOFCs as power sources for electric vehicles and portable devices, and poses serious problems on their structural design.

^{*} Corresponding author. Tel.: +98 21 77240540; Fax: +98 21 77240488
E-mail address: mnouri@iust.ac.ir (N.M. Nouri)

In order to overcome the problems associated with planar SOFCs, much of the recent efforts are devoted to develop new materials and configurations to improve the performance at reduced operating temperatures. By lowering the operating temperature of SOFC to around 700°C, the majority of the problems associated with planar SOFC can be resolved. However, the ionic conductivity of the electrolyte decreases with the reduction of operating temperature. The reduction in ionic conductivity of the electrolyte resulting in higher ohmic overpotential at reduced operating temperatures can be minimized by either using electrode (anode or cathode) supported configuration of SOFC, wherein thin electrolytes of thicknesses in the range of 10-20 μm are deposited on the thick electrode (anode or cathode) or using composite ceramic electrolyte in an electrolyte supported configuration having high ionic conductivity at reduced temperatures [2].

Mathematical modeling is an essential aspect of SOFC technology development process. A numerical model facilitates research and development by minimizing the need of repetitive and costly experimentation. Numerical simulation of SOFCs provides a thorough understanding of how cell performance is affected by various operating and design parameters such as pressure, TPB length, pore size, porosity, thickness of various components, and ionic and electronic conductivities of ion-conducting and electronic-conducting particles of the electrode, respectively, and thus helps in optimizing cell and stack design.

Numerous models of SOFCs exist in the literature [5, 8-10, 13-15], varying in the number of assumptions employed. The common assumption in the existing SOFC models is the consideration of reaction zone layers as mathematical elements, treating them as boundary conditions. However, for composite electrodes such as those in SOFCs, the reaction zone layers are spreaded out into the electrode some distance (10-15 μm) from the electrolyte/electrode interfaces [16-18]. Reaction zone layers are relatively thin layers where fuel and oxidant are electrochemically converted into electrical work, heat and water vapor.

The objective of the present study is to develop a mathematical model and to use FEM for solving the governing equations. The FEM numerical results are validated against the measured performance data and compared with CVM results available in the literature [5] and the experimental data. Finally, the effect of various operating and design parameters on the performance of SOFC is investigated.

2. Model formulation

Fig. 1 illustrates different layers of SOFC. A conventional SOFC consists of three major layers such as anode electrode layer, electrolyte layer and cathode electrode layer. Two additional layers, as shown in Fig. 1, located between the anode electrode layer and electrolyte layer and cathode electrode layer and electrolyte layer are called anode reaction zone layer and cathode reaction zone layer, respectively. The reaction zones on either side of the electrolyte are considered to be distinct layers because of the fact that the electrochemical reaction not only occurs on the interface between the anode and the electrolyte, and the cathode and the electrolyte but also extends to a depth of 10-15 μm inside electrode layers [16-18].

The cell is assumed to operate under steady state condition and the parameters vary in the x-direction only, as shown in Fig. 1. The temperature and total pressure are assumed to be uniform in the porous electrode and reaction zone layers. The cell uses pure hydrogen as a fuel. The reactant gas mixtures are approximated as ideal gases with negligible viscous, Soret, Dofour and gravity effects. Since the reaction zone layers are considered as separate regions, there are no electrochemical reactions (either oxidation or reduction) in the electrode layers. The reaction zone layers consist of mixture of electron-conducting particles, ion-conducting particles and void space occupied by gaseous species. The electrolyte layer is assumed to be a dense solid with no interconnected porosity. With these assumptions the governing equations and constitutive equations used in this model are described in Tables 1-5 and Table 6, respectively. The TPB length specific transfer current densities of Eqs. (13) and (14) are the empirical equations derived

by Bieberle et al [19] and Radhakrishnan et al [20]. Radiation is not considered due to minor effect on planar-type SOFCs as described by Daun et al [21]. More detailed description of the equations can be found in COMSOL user guide [22]. Binary diffusion coefficients can be calculated using the Fuller-Schettler-Giddings formula (Eq. 16) [7]. In this equation ν_i is atomic diffusion volume. Values of ν_i used in this equation are in Table 7.

Table 1

Governing equations for anode electrode (backing) layer.

Conservation of species	$\nabla \left(-\rho \omega_i \sum D_{ij}^{eff} \left(\nabla x_i + (x_i - \omega_i) \frac{\nabla p}{p} \right) + \rho \omega_i \mathbf{u} \right) = \mathbf{0} \quad (1)$
Conservation of electronic charge	$\nabla \cdot (-\sigma_{bl}^{eff} \nabla \varphi_{el}) = 0 \quad (2)$
Conservation of ionic charge	-

Table 2

Governing equations for cathode electrode (backing) layer.

Conservation of species	$\nabla \left(-\rho \omega_i \sum D_{ij}^{eff} \left(\nabla x_i + (x_i - \omega_i) \frac{\nabla p}{p} \right) + \rho \omega_i \mathbf{u} \right) = \mathbf{0} \quad (3)$
Conservation of electronic charge	$\nabla \cdot (-\sigma_{cl}^{eff} \nabla \varphi_{el}) = 0 \quad (4)$
Conservation of ionic charge	-

Table 3

Governing equations for anode reaction zone layer.

Conservation of species	$\nabla \left(-\rho \omega_i \sum D_{ij}^{eff} \left(\nabla x_i + (x_i - \omega_i) \frac{\nabla p}{p} \right) + \rho \omega_i \mathbf{u} \right) = \mathbf{0} \quad (5)$ Where, $= -S_{H_2O} = -\frac{i_{TPB}^A}{2F} M_{H_2} (\text{or } H_2O)$
Conservation of electronic charge	$\nabla \cdot (-\sigma_{rl}^{eff} \nabla \varphi_{el}) = i_{TPB}^A \cdot \lambda_{TPB} \quad (6)$
Conservation of ionic charge	$\nabla \cdot (-\kappa_{rl}^{eff} \nabla \varphi_{io}) = -i_{TPB}^A \cdot \lambda_{TPB} \quad (7)$

Table 4

Governing equations for cathode reaction zone layer.

Conservation of species	$\nabla \left(-\rho \omega_i \sum D_{ij}^{eff} \left(\nabla x_i + (x_i - \omega_i) \frac{\nabla p}{p} \right) + \rho \omega_i \mathbf{u} \right) = S_i$ <p style="text-align: center;">Where, $= -\frac{i_{TPB}}{4F} M_{O_2}$ and $S_{N_2} = 0$</p>	(8)
Conservation of electronic charge	$\nabla \cdot (-\sigma_{rl}^{eff} \nabla \varphi_{el}) = i_{TPB} \cdot \lambda_{TPB}$	(9)
Conservation of ionic charge	$\nabla \cdot (-\kappa_{rl}^{eff} \nabla \varphi_{io}) = -i_{TPB} \cdot \lambda_{TPB}$	(10)

Table 5

Governing equations for electrolyte layer.

Conservation of species	-	
Conservation of electronic charge	-	
Conservation of ionic charge	$\nabla \cdot (-\kappa \nabla \varphi_{io}) = 0$	(11)

Mass flow rates of hydrogen, water and oxygen species are calculated by Eqs. (5) and (8), which sum the molar fluxes due to fluid flow and diffusion in the respective anode and cathode compartments [6]. Diffusion in porous media is usually described by a molecular (particle-particle collision) and/or a Knudsen (particle-wall collision) diffusion mechanism [6]. In order to account for a detailed diffusion mechanism, both modes have been considered by implementing the Dusty Gas Model (DGM). The DGM is derived by considering the solid matrix as large stationary spheres suspended in the gas mixture. The DGM diffusivity is then given by Eq. (18) [6].

2-1 Boundary conditions

The location at which boundary conditions are needed to complete the mathematical formulation are illustrated in Fig. 1 as “a”, “b”, “c”, “d”, “e” and “f”. Locations “a” and “f” are the interfaces between the fuel channel and the anode electrode (backing) layer and the air channel and the cathode electrode (backing) layer, respectively; the boundary conditions at these locations are specified boundary conditions, where the composition of gaseous species and electronic potential are specified. The boundary conditions at the interfaces between the anode electrode and the anode reaction zone layers (location “b”) and the cathode electrode and the cathode reaction zone layers (location “e”) are continuous flux boundary conditions for gaseous species and electronic potential, where the diffusion flux and electronic current density are continuous, whereas insulated boundary condition for ionic potential, which implies ionic current density is zero.

Table 6
Constitutive equations.

Constitutive equations	Mathematic equations
Open circuit voltage	$V^{OCV} = \frac{247340 - 54.85T}{2F} + \frac{R_g T}{2F} \left(\frac{p_{H_2}}{p_{H_2O}} \left(\frac{p_{O_2}}{100000} \right)^{\frac{1}{2}} \right) \quad (12)$
TPB length specific transfer current density of anode reaction zone layer	$i_{TPB}^A = \frac{-\eta_A}{1.645 \times 10^{-4} \eta_A p_{H_2}^{-0.11} 14000^{-0.67} \exp(10212/T)} \quad (13)$
TPB length specific transfer current density of cathode reaction zone layer	$i_{TPB}^C = \frac{RT \exp((2F/RT)\eta_C) - \exp(-(2F/RT)\eta_C)}{4F \cdot 0.00136 p_{O_2}^{-0.25} \exp(17401/T)} \quad (14)$
TPB length	$\lambda_{TPB} = 6\pi d_p n_t \frac{Z_{io} Z_{el}}{6} P_{el} P_{io} \sin \frac{\theta}{2} \quad (15)$
Binary diffusivity	$D_{ij} = \frac{0.00143T^{1.75}}{p \left(\frac{M_i + M_j}{M_i M_j} \right)^{1/2} (v_i^{1/2} + v_j^{1/2})^2} \quad (16)$
Knudsen diffusivity	$D_{ik} = \frac{97}{2} d_{pore} \sqrt{\frac{T}{M_i}} \quad (17)$
Effective diffusion coefficient	$D_{ij}^{eff} = \frac{s}{\tau} \left(\frac{1}{D_{ij}} + \frac{1}{D_{iK}} \right)^{-1} \quad (18)$
Density	$\rho = \frac{p}{R_g T} \sum_i x_i M_i \quad (19)$
Total number of particles per unit volume	$n_t = \frac{1 - \varepsilon}{(4/3)\pi r_{el}^3 (n_{el} + (1 - n_{el})(r_{io}/r_{el})^3)} \quad (20)$
Number fraction of electron conducting particles	$n_{el} = \left[\frac{\phi}{\phi + (1 - \phi)(r_{io}/r_{el})^3} \right] \quad (21)$
Number fraction of ion conducting particles	$n_{io} = 1 - n_{el} \quad (22)$
Coordination number of electron conducting particles	$Z_{el} = 3 + \left[\frac{3}{n_{el} + (1 - n_{el})(r_{io}/r_{el})^2} \right] \quad (23)$

$$\text{Coordination number of ion conducting particles} \quad Z_{io} = 3 + \frac{3 \times (r_{io} / r_{el})^2}{n_{el} + (1 - n_{el})(r_{io} / r_{el})^2} \quad (24)$$

$$\text{Probabilities of electron conducting particles} \quad P_{el} = \left[1 - (2 - Z_{el-el} / 2)^{2.5} \right]^{0.4}$$

$$\text{Where, } Z_{el-el} = \frac{n_{el} Z_{el}^2}{6} \quad (25)$$

$$\text{Probabilities of ion conducting particles} \quad P_{io} = \left[1 - (2 - Z_{io-io} / 2)^{2.5} \right]^{0.4}$$

$$\text{Where, } Z_{io-io} = \frac{n_{io} Z_{io}^2}{6} \quad (26)$$

$$\text{Effective electronic conductivity of the backing layers} \quad \sigma_{bl}^{eff} = \left(\frac{1 - \varepsilon}{\tau} \right) \sigma \quad (27)$$

$$\text{Effective electronic conductivity of the reaction zone layers} \quad \sigma_{rl}^{eff} = \phi \left(\frac{1 - \varepsilon}{\tau} \right) \sigma \quad (28)$$

$$\text{Effective ionic conductivity of the reaction zone layers} \quad \kappa_{rl}^{eff} = (1 - \phi) \left(\frac{1 - \varepsilon}{\tau} \right) k \quad (29)$$

At locations “c” and “d”, the interfaces between the anode reaction zone layer and the electrolyte layer, and the cathode reaction zone layer and the electrolyte layer, the diffusion flux and electronic current density are zero, whereas the ionic current density is continuous and is equal to the total current density. Mathematically, the boundary conditions at different locations in Fig. 1 are listed in Table 8.

Table 7

Diffusion volumes for simple molecules [7].

H ₂	7.07
N ₂	17.9
O ₂	16.6
H ₂ O	12.7

2-2 Numerical procedures

The finite element commercial package, COMSOL 3.4, was used to solve a set of governing equations. The application modes of COMSOL multiphysics and chemical engineering module were employed which are provided in the software. A parametric nonlinear solver with direct linear system solver was adopted for the calculations of a highly non-linear problem. The convergence was judged by the relative tolerance criteria of 1×10^{-6} . The damping parameters and scaling of dependent variables were manually tuned to improve convergence and to save calculation costs. The structured and uniform grid cells were established. Number of elements for the calculations was equal to 2236.

Table 8
Boundary conditions.

Location of x	“a” and “f”	“b” and “e”	“c” and “d”
Conservation of species	= specified	$N_i _{b_l} = N_i _{r_l}$	$N_i = 0$
Conservation of electronic charge	= specified	$J_e _{b_l} = J_e _{r_l}$	$J_e = 0$
Conservation of ionic charge	–	$J_i = 0$	$J_i _{b_l} = J_i _{r_l}$

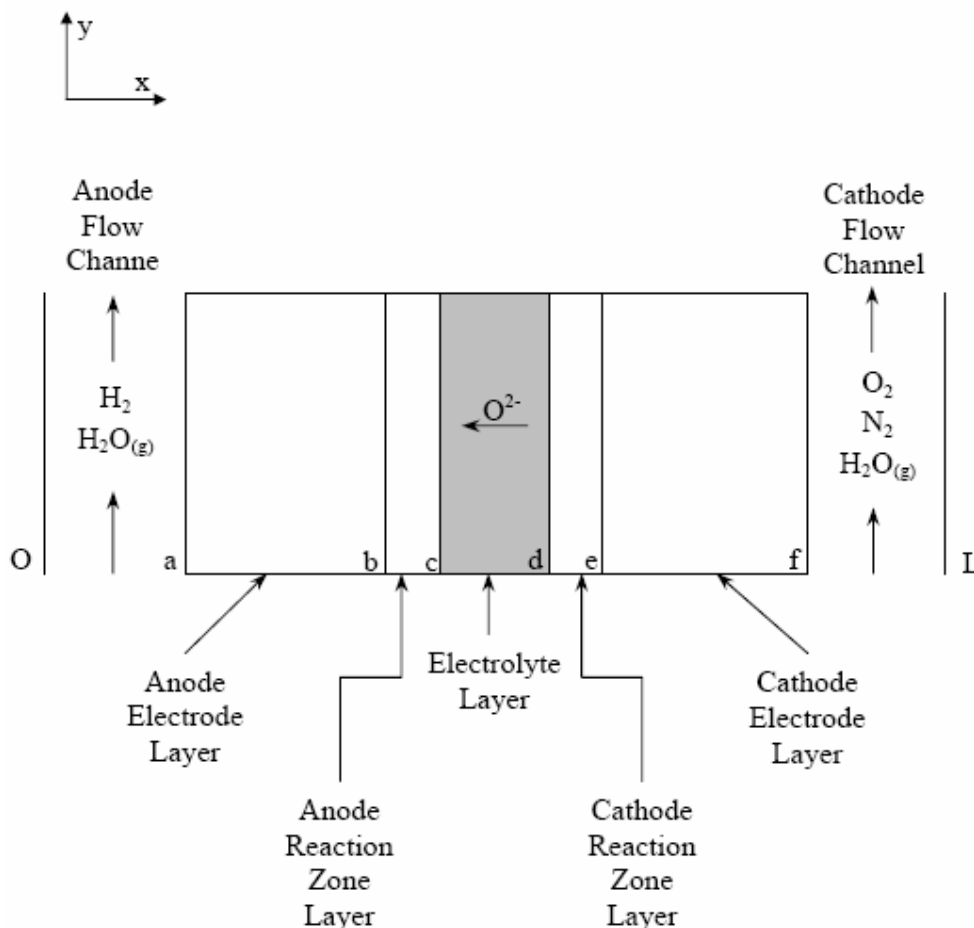


Fig. 1. Illustration of different layers of solid oxide fuel cell.

2.3. Model validation

Using the parameters listed in Table 9, the predicted cell performance is compared with the experimental data and CVM found in the literature [11] and [5] respectively, and is shown in Fig. 2. The performance of the cell is predicted when the cell is supplied with 95% H₂ and 5% H₂O as fuel, operating at a temperature and pressure of 1073K and 1atm, respectively. Oxygen composition in the ambient air is used as oxidant. The R²-value, an indicator between 0 and 1, reveals how closely the predicted values correspond to the experimental data, is obtained for the Hussain et al’s model as 0.988 and for the present model as 0.996 that shows the present model predictions agree with the experimental results better than CVM results.

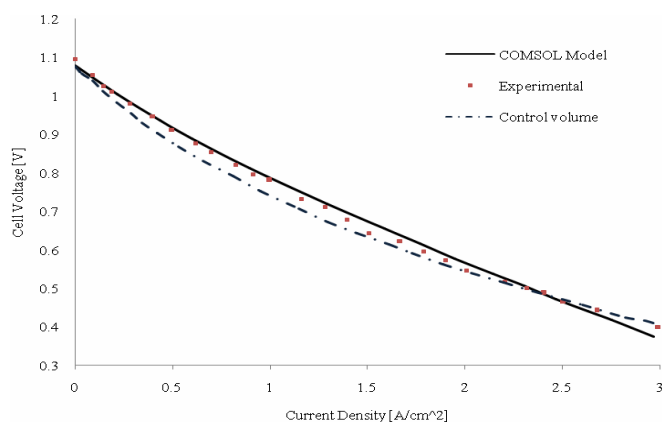


Fig. 2. Comparison between the model predictions and experimental results of Rogers et al. [11].

It is worth mentioning that all the parameters used in the model validation are obtained from Rogers et al [11] except the value of tortuosity. The value of tortuosity is varied to obtain the best agreement between the present model predictions and the experimental results shown in Fig. 2, since the value reported by Rogers et al [11] is unity. The typical tortuosity value for SOFC electrodes is in the range of 2–6 [4]. Hence, the tortuosity value of 2.75 used in the present model predictions is in the typical range for SOFC electrodes and provides the best agreement with the experimental results [5].

3. Results and discussions

The developed SOFC model can be used to investigate the effect of operating and design parameters on the cell performance. Oxygen composition in the ambient air is used as oxidant. the results shown are based on parameters listed in Table 9.

Fig. 3 shows the effect of pressure on the performance of the cell. The temperature and other parameters are set as parameters listed in Table 9. It can be observed that increasing the pressure not only increases the reversible cell potential but also increases the actual cell potential. With the increase of pressure, the reactant concentration at the reaction sites increases, which in turn enhances the rate of electrochemical reaction and rate of mass transport resulting in the minimization of anode and cathode overpotentials and hence better performance. However, increase in pressure results in other problems such as limitation on material selection, gas sealing and mechanical strength of the cell components [5].

The effect of porosity on the performance of the cell is shown in Fig. 4. The temperature and pressure were set at 1073K and 1atm respectively, and all other parameters are the same as that of parameters given in Table 9.

Table 9

Parameters used for model.

Operating temperature, T_{op} (K)	1073
Total pressure, p (atm)	1
Fuel composition,	0.95; 0.05
Air composition,	0.21; 0.79
Anode conductivity, σ (Sm^{-1})	71428.57
Cathode conductivity, σ (Sm^{-1})	5376.34
Electrolyte conductivity, κ (Sm^{-1})	0.64
Anode electrode layer thickness (μm)	1000
Cathode electrode layer thickness (μm)	50
Anode reaction zone layer thickness (μm)	20
Cathode reaction zone layer thickness (μm)	20
Electrolyte thickness (μm)	10
Porosity of anode and cathode, ε	0.375
Tortuosity of anode and cathode, τ	2.75
Pore diameter of anode and cathode, d_p (μm)	1.5
Contact angle between electron and ion conducting particles θ ($^\circ$)	15
Radius of electron conducting particles, r_{el} (μm)	0.1
Radius of ion conducting particles, r_{io} (μm)	0.1
Volume fraction of electron conducting particles, Φ	0.5
Reference H_2 concentration, (molm^{-3})	10.78
Reference O_2 concentration, (molm^{-3})	2.38
Reference exchange current density for H_2 oxidation, i_{0f} (Am^{-2})	1320
Reference exchange current density for O_2 oxidation, i_{0r} (Am^{-2})	400
Reaction order for H_2 oxidation,	0.5
Reaction order for O_2 reduction,	0.5

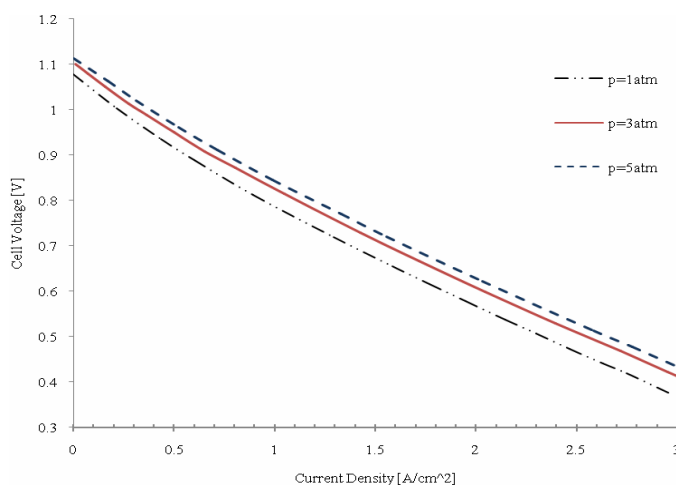


Fig. 3. Effect of pressure on cell performance.

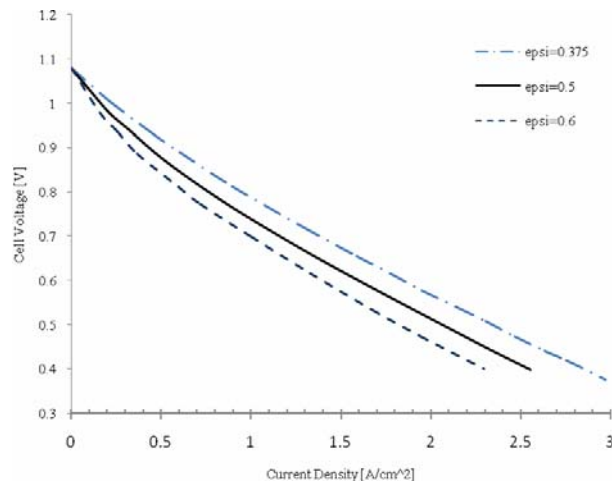


Fig. 4. Effect of porosity on cell performance

It can be seen that increasing the porosity of the cell components decreases the cell performance. Increasing the porosity increases the void fraction and decreases the solid fraction of the porous layers resulting in the reduction of the active surface area available for the electrochemical reaction. Moreover, the effective ionic and electronic conductivities of the porous layers decrease with the increase of porosity, which results in the increase of ohmic overpotential. Although the concentration overpotential decreases with the increase of porosity due to the increased mass transport rates but the cell performance decreases due to increased ohmic overpotential with porosity.

Fig. 5 depicts the effect of tortuosity on cell performance. The temperature and pressure were again set at 1073K and 1atm respectively. It can be observed that increasing the tortuosity of the porous layers decreases the performance of the cell. Increasing the tortuosity of the porous layers means increasing the tortuous path, which adds additional resistance to the reactant species diffusing through the porous layers resulting in the reduction of reactant concentration at the reaction sites and thereby decreasing the rate of electrochemical reaction. In addition, the effective ionic and electronic conductivities decrease with the increase of tortuosity resulting in

the increase of ohmic overpotential and hence cell performance decreases with the increase of tortuosity.

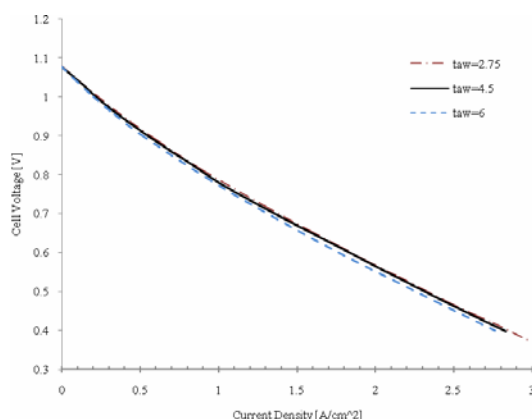


Fig. 5. Effect of tortuosity on cell performance.

4. Conclusions

A mathematical model of solid oxide fuel cell (SOFC) has been developed, which can predict the performance at various operating and design conditions. The important feature of this model is to compare Finite Element method (FEM) and Control Volume method (CVM) obtained by Hussain et al with the experimental data. It was found that the results obtained from the current model show more accurate agreement with the experimental data in comparison with the results obtained by Hussain et al. In addition, micro characteristics of the electrodes are incorporated into the model. Moreover, the effect of operating and design conditions on the cell performance has been examined. It was found that increasing the pressure and decreasing the porosity and the tortuosity of the porous layers increase the cell performance.

Nomenclature

\mathbf{u}	Velocity vector (m s^{-1})
D_{ij}	Binary diffusion coefficient ($\text{m}^2 \text{s}^{-1}$)
x_i	Mole fraction of species i
\dot{S}_i	Rate of production or consumption of species i ($\text{kg m}^{-3} \text{s}^{-1}$)
M_i	Molecular weight of species i (mol kg^{-1})
F	Faraday's constant (96487 C mol^{-1})
p	Total pressure (Pa)
i_{TPB}	TPB length specific transfer current density (A m^{-2})
V^{cell}	Cell voltage (V)
V^{OCV}	Open circuit voltage (V)
T	Operating temperature (K)
R_g	Universal gas constant ($8.314 \text{ J K}^{-1} \text{ mol}^{-1}$)
P_{el}	Probabilities of electron conducting particles
P_{io}	Probabilities of ion conducting particles
d_p	Diameter of spherical particle (m)
n_t	Number density of total particles
Z_{el}	Coordination number of electron conducting particles
Z_{io}	Coordination number of ion conducting particles
D_{iK}	Knudsen diffusivity ($\text{m}^2 \text{s}^{-1}$)
d_{pore}	Pore diameter (m)

r_{el}	Radius of electron conducting particles (m)
r_{io}	Radius of ion conducting particles (m)
n_{el}	Number fraction of electron conducting particles
n_{io}	Number fraction of electron conducting particles
<i>Greek symbols</i>	
φ	Potential (V)
σ	Electronic conductivity ($S\ m^{-2}$)
κ	Ionic conductivity ($S\ m^{-2}$)
ρ	Density ($kg\ m^{-3}$)
ω_i	Mass fraction of species i
λ_{TPB}	TPB length ($m^3\ m^{-2}$)
η	Overpotential (V)
θ	Contact angle between electron and ion conducting particles
v_i	Atomic diffusion volume for species i ($m^3\ mol^{-1}$)
ε	Porosity
τ	Tortuosity
ϕ	Volume fraction of electron conducting particles
<i>Subscripts</i>	
<i>bl</i>	Electrode (backing) layer
<i>rl</i>	Reaction zone layer
<i>el</i>	electronic
<i>io</i>	ionic
<i>TPB</i>	Three phase boundary
<i>Superscripts</i>	
<i>eff</i>	Effective
<i>A</i>	Anode
<i>C</i>	Cathode

References

- [1] S.C. Singhal, K. Kendall, High Temperature Solid Oxide Fuel Cells Fundamentals Design and Applications, Kidlington Oxford, Elsevier, 2003.
- [2] J. Yuan, B. Sunden, Trans. ASME J. Heat Transfer 127 (2005) 1380-1390.
- [3] J. Larminie, A. Dicks, Fuel Cell Systems Explained. 2th ed, John Wiley and Sons Ltd, West Sussex, England, 2003.
- [4] M.M. Hussain, Multi-Component and Multi-Dimensional Mathematical Modeling of Solid Oxide Fuel Cells. PhD Thesis, University of Waterloo, 2008.
- [5] M.M. Hussain, X. Li, I. Dincer, J. Power Sources 161 (2006) 1012-1022.
- [6] R. Taylor, R. Krishna, Multi Component Mass Transfer, John Wiley, 1993.
- [7] R. Perry, D. Green, Perry's Chemical Engineering Handbook, 7th ed., McGraw-Hill, 1997.
- [8] N. Akhtar, S.P. Decent, D. Loghin, K. Kendall, Inter. J. Hydrogen Energy (2009) 1-19.
- [9] D.H. Jeon, Electrochim. Acta 54 (2009) 2727-2736.
- [10] P. Costamagna, P. Costa, V. Antonucci, Electrochim. Acta 43 (1998) 375-394.
- [11] W.A. Rogers, R.S. Gemmen, C. Johnson, M. Prinkey, M. Shahnam, Fuel Cell Sci. Eng. Technol. ASME (2003) 517-52.
- [12] K. Tseronis, I. Kookos, K. theodoropoulos, Modeling and design of the solid oxide fuel cell anode, COMSOL Users conference, Birmingham (2006).
- [13] K. Nikooyeh, A.A. Jeje, J. M. Hill, J. Power Sources 171 (2007) 601-609.
- [14] Y. Mollayi Barzi, M. Ghassemi, M.H. Hamed, J. Power Sources 192 (2009) 200-209.
- [15] S. Liu, W. Kong, Z. Lin, J. Power Sources 194 (2009) 854-863.
- [16] C.W. Tanner, K.Z. Fung, A.V. Virkar, J. Electrochem. Soc. 144 (1997) 21-30.
- [17] W. Lehnert, J. Meusinger, F. Thom, J. Power Sources 87 (2000) 57-63.
- [18] J. Fleig, Annu. Rev. Mater. Res. 33 (2003) 361-382.
- [19] A. Bieberle, L.P. Meier, L.J. Gauckler, J. Electrochem. Soc. 148 (2001) A646-A656.

- [20] R. Radhakrishnan, A.V. Virkar, S.C. Singhal, *J. Electrochem. Soc.* 152 (2005) A927-A936.
- [21] K.J. Daun, S.B. Beale, F. Liu, G.J. Smallwood, *J. Power Sources* 157 (2006) 302-310.
- [22] COMSOL User Guide, COMSOL Inc., Burlington, MA, (2005).